Journal of Mathematical Imaging and Vision 21: 205–223, 2004

Shape Restoration via a Regularized Curvature Flow

DEBORA GIL AND PETIA RADEVA
Computer Vision Center (CVC), Edifici O, Campus UAB, 08193 Bellaterra, Barcelona, Spain
debora@cvc.uab.es
petia@cvc.uab.es

Abstract. Any image filtering operator designed for automatic shape restoration should satisfy robustness (whatever the nature and degree of noise is) as well as non-trivial smooth asymptotic behavior. Moreover, a stopping criterion should be determined by characteristics of the evolved image rather than dependent on the number of iterations. Among the several PDE based techniques, curvature flows appear to be highly reliable for strongly noisy images compared to image diffusion processes.

In the present paper, we introduce a regularized curvature flow (RCF) that admits non-trivial steady states. It is based on a measure of the local curve smoothness that takes into account regularity of the curve curvature and serves as stopping term in the mean curvature flow. We prove that this measure decreases over the orbits of RCF, which endows the method with a natural stop criterion in terms of the magnitude of this measure. Further, in its discrete version it produces steady states consisting of piece-wise regular curves. Numerical experiments made on synthetic shapes corrupted with different kinds of noise show the abilities and limitations of each of the current geometric flows and the benefits of RCF. Finally, we present results on real images that illustrate the usefulness of the present approach in practical applications.

Keywords: non-linear filtering, geometric flows, shape restoration

1. Introduction

Over the past 15 years, many algorithms to enhance and smooth images have been developed; most of them are governed by a parabolic partial differential equations (PDE) having the image to be filtered as initial condition. This fact confers the associated image operator several sensible properties (causality, local comparison principle and regularity) as well as enables the use of mathematical tools in order to study their behavior in terms of the differential operator involved in the equation [1, 20]. From this point of view, one can split the current image operators into two distinct families: the ones arising from heat diffusion processes, which can be written in divergence form, and the ones based on geometric flows.

The first group, that includes Gaussian filtering, edge enhancement of Perona and Malik [19], anisotropic diffusion [23], image selective smoothing [3] and half-quadratic minimization [2] among others, filters an image by means of a PDE that describes a physical process of heat diffusion. Hence, they must always treat image edge blurring. The most efficient solution up to now consists in including a term preventing diffusion across edges. This implies the choice of a threshold value determining what magnitude of the image gradient is to be considered an edge and constitutes a main problem when dealing with highly noisy images.

The other group contains the mean curvature flow [10] and the min-max flow [14]. Its main feature consists in that the PDE that governs the image smoothing relies exclusively on the geometry of the level curves of the image. Hence, it does not produce any edge blurring, which makes these techniques more robust in very noisy images. The highly non-linearity of the PDE and the fact of being of Hamilton-Jacobi type [7] may imply the formation of shocks during the image evolution. Therefore, solutions must be understood

in the viscosity sense [4, 6, 7, 18], complicating the numerical integration of the equations. In [18] it is proved that an explicit finite difference scheme is a suitable way to integrate such equations. Explicit schemes have the inconvenience of requiring possibly small time steps to ensure convergence. In diffusion processes, for instance, it depends on the coefficients of the diffusion tensor [26] and large time steps are not advisable.

Another usual drawback of most of the present image filtering techniques is that their steady-state is trivial, that is a constant image for diffusion processes [24] and either a point or a straight line for curvature based ones [8, 10, 13]. This property, although desirable for a scale-space analysis of images/shapes [1, 12], is a main nuisance when using these techniques for segmenting purposes, as they require a stopping time to recover shapes of interest. Half-quadratic minimization and the min/max flow are two recent techniques used to cope with this problem. The technique we introduce in the present paper is also on this line of research.

The method we propose consists of curvature evolution image process where the shapes should present minimal variation of curvature instead of penalizing curvature magnitude. In this context, our evolution process is called regularized curvature flow (RCF). A second and important feature of the RCF is that it achieves non trivial steady states (compared to other techniques where the asymptotic solution is a point of the image). To this purpose, we introduce a roughness function, that measures the local irregularity of a curve in terms of the smoothness of its tangent direction along the curve. By incorporating the roughness measure to the mean curvature flow, RCF succeeds in taking benefit of the smoothing effect of the mean curvature flow until the roughness function cancels. In this manner, we obtain steady curves conserving features significant enough to identify the original noisy shape. Numerically, the equation can be integrated via the level sets formulation using a finite difference Euler scheme that supports large time steps compared to diffusion processes.

The paper covers the following items. In Section 2 we give an overview on the most used recently developed techniques in image filtering, with a especial emphasis on their properties concerning image processing. Next, there is a detailed description of the method proposed, the roughness measure is defined in Section 3 and RCF is formulated in Section 4. Finally, in Section 5, we present numerical experiments on synthetic shapes and real images.

2. Review of Existing Techniques

Let us begin with a short overview of the formulation and properties of the most popular and recent techniques for image processing. We have split them into two main families: diffusion processes and geometric flows.

2.1. Diffusion Processes

This group of filtering operators are based on the physical process of heat diffusion. The image to be smoothed is the initial heat distribution, whose evolution in time is given by the PDE:

$$u_t = \operatorname{div}(T \cdot \nabla u)$$

where T is a positive definite 2×2 matrix, known as the diffusion tensor, that determines at each pixel/point the direction towards heat spreads.

(a) Edge Enhancement Diffusion of Perona-Malik. This method, introduced by Perona and Malik in [19], not only overcomes edge blurring but also enhances edges and profits from the smoothing effects of the Gaussian filtering at image regions where contrast changes are not significant enough. The image operator they propose follows:

$$u_t = \operatorname{div}(g(|\nabla u|)\nabla u) = g u_{\xi\xi} + (g + g'|\nabla u|)u_{\eta\eta} \quad (1)$$

where $\xi = \frac{\nabla u^{\perp}}{|\nabla u|}$, $\eta = \frac{\nabla u}{|\nabla u|}$ and $g(s) = \frac{\lambda^2}{\lambda^2 + s^2}$ is the edge enhancing function. In physical terms, one can understand the function g as a stopping diffusion factor that prevents diffusion across edges. In this sense only edges such that $|\nabla u| < \lambda$ are blurred and, further, at those points where $g + g'|\nabla u| < 0$ edges are enhanced.

The above properties constitute the main drawbacks of the technique. Backwards diffusion makes the method potentially ill-posed [24, 28] (though finite differences work fine [25]) and produces step images (Stair-Casing Effects, [27, 28]). Incomplete edges in real images are prone to be blurred (Pinhole Effect [17]). The most popular solution is the anisotropic diffusion [23].

(b) Anisotropic Diffusion of Weickert. This method consists in using a regularized version of the gradient:

$$u_t = \operatorname{div}(D(J_\rho(\nabla u_\sigma))\nabla u) \quad (2)$$

where the diffusion tensor $D(J_\rho(\nabla u_\sigma))$ has equal eigenvectors than the Structure Tensor, J_ρ, of the image with eigenvalues depending on the structures to be enhanced.

By general arguments on parabolic PDE's [3, 23] we have that, as far as $D(J_\rho)$ is positive definite, the initial boundary problem has a unique smooth solution which tends asymptotically [24] towards a constant function. This is the main drawback of the method, since it implies the need of a stopping time if any image features are to be preserved.

2.2. Geometric Flows

The other family of filtering operators are those based on the evolution of the level curves of the image under a function of their curvature. If $\gamma_0(u)$ is a plane curve, its evolution under a generic curvature flow is the solution to the PDE given by:

$$\gamma_t(u,t) = g(\kappa)\vec{n} \quad \text{with} \quad \gamma(u,0) = \gamma_0(u) \tag{3}$$

where $\vec{n}$ denotes the curve unit normal and κ its curvature. In order to guarantee that the original shape γ_0 will be smoothed, the total Gaussian curvature, $\bar{\kappa}(t) = \int_0^1 |\kappa|\sqrt{\dot{x}^2 + \dot{y}^2}du$, and the number of inflexion points must decrease in time.

Since the quantities involved in (3) are geometrically intrinsic and a change of parameter does not affect the shape of the solution, geometric flows can be applied to image filtering via an implicit level-sets formulation [15, 21]:

$$u_t = |\nabla u| g\left(\operatorname{div}\left(\frac{\nabla u}{|\nabla u|}\right)\right) = |\nabla u| g(u_{\xi\xi})$$

Due to the absence of the second derivative $u_{\eta\eta}$, curvature flows are contrast preserving [1]. This is their main advantage over diffusion processes [11, 15], as they modify the shapes of edges without blurring.

(a) Mean Curvature Flow. This flow, also known as Geometric Heat Equation, is one of the most widely studied geometric flows. We remit the reader to [8, 10, 13] for a detailed study of the properties, we will enumerate. Its formulation for curves is given by:

$$\gamma_t(u,t) = \kappa\vec{n} \tag{4}$$

In [10] it is shown that, as far as the curvature remains bounded, a smooth solution exists. This solution fulfills the necessary conditions to smooth irregularities:

Proposition 2.1 [13]. *Let $\gamma(u,t)$ be a solution of (4) for $t \in [0,T)$ and $u \in [0,1]$. Then, the total Gaussian curvature, $\bar{\kappa}(t) = \int_0^1 |\kappa|\sqrt{\dot{x}^2 + \dot{y}^2}du$ is a decreasing function of time,*

$$\bar{\kappa}(t) \leq \bar{\kappa}(0)$$

The equality holds if and only if the initial curve is convex.

Proposition 2.2 [10]. *The number of inflexion points (i.e. zeros of the curvature) of a family of curves, $\gamma(u,t)$, satisfying (4) for $t \in [0,T)$ is a non-increasing function of time.*

Besides, we have a complete description of the asymptotic behavior for the family fulfilling (4) in this Proposition:

Proposition 2.3 [8, 10]. *The solution to (4) becomes a circle and finally collapses to a point.*

This Proposition supplies images and curves evolving under the curvature flow with a desirable property for a scale-space analysis [1, 12], which studies images/shapes at different level of detail by means of a progressive simplification of their shapes and features. However, as in the case of diffusion processes, this property represents a main drawback because it implies a stopping time in order to preserve enough features as to recognize the original shapes in the image.

The first ones to address successfully the problem were Malladi and Sethian [14] with their:

(b) Min/Max Flow.

$$u_t = \begin{cases} \min(\kappa, 0) & \text{if } \Phi(x,y) < \upsilon \\ \max(\kappa, 0) & \text{if } \Phi(x,y) \geq \upsilon \end{cases} \tag{5}$$

where $\Phi(x,y)$ is the average of all pixel values in a window centered at (x,y) and υ is the mean value in the window on the level curve to be smoothed. The steady state of the equation is a polygonal curve.

The former theoretical analysis of recent filtering techniques points out that if an image smoothing operator is to be robust against strong noisy images, it should be independent of image intensity. Essential advantage in this context is represented by geometric flows. However, curvature based flows penalize high curvature regardless of their regularity. Notice that descriptors of shapes depend significantly on the extreme

values of the curvature of the contours. Only points lying in a neighborhood of high variability in the curvature are prone to be consequence of noise and should be smoothed. Hence, an operator designed with shape recognition purposes should include a term penalizing irregularity in the curvature rather than its magnitude. We propose a geometric flow that includes a function that measures the degree of local irregularity present in the curve.

3. A Measure of Shape Irregularities

We model noise or lack of regularity in a curve by means of the variability of its normal unit vector $\vec{n}$ around each point. We compute this variability as the projection of the unit normal onto a robust mean of the unit normal in a neighborhood of each point. In order to obtain a robust mean of the normal unit vector we use the structure tensor. We define the structure tensor J_ρ of the unit normal as the convolution of the projection matrices onto the vector space generated by $\vec{n}$ with an one dimensional gaussian, G_ρ, of variance ρ and zero mean:

$$\begin{aligned} J_\rho(u) &= (G_\rho * (\vec{n} \otimes \vec{n}))(u) = (G_\rho * (\vec{n}\vec{n}^T))(u) \\ &= \begin{pmatrix} a_{11}(u) & a_{12}(u) \\ a_{12}(u) & a_{22}(u) \end{pmatrix} \\ J_\rho(u) &= \int_{-\infty}^{\infty} G_\rho(\tilde{u} - u)(n(\tilde{u}) \otimes n(\tilde{u}))\, d\tilde{u} \end{aligned} \tag{6}$$

The above quantity hinges on the parameter u taken along the curve. This is a natural consequence of considering any smooth approximation of a function. However, as it stands, J_ρ is nothing but the solution to the heat equation with initial condition the projection matrix $n \otimes n$ at time $t = \rho$. This confers a geometric flow including the roughness measure as stopping term interesting properties from an image processing point of view because it ensures convergence to non trivial images. Furthermore, these **properties are not altered by a change of parameter**. Since RCF asymptotic behavior depends on them, our measure of irregularity will be based on the structure tensor given by (6).

We recall that the symmetric matrix J_ρ is positive semi definite, and therefore it diagonalizes in a basis of orthonormal vectors, v_1, v_2. The eigenvector of maximum eigenvalue, $v_1 = (\cos\psi, \sin\psi)$, is a robust mean of the unit normal. In the absence of noise, the scalar product $\langle v_1, \vec{n} \rangle$ is close to one. Since, in fact, it is the cosine of the angle between v_1 and $\vec{n}$, the sine, $\sin(\psi - \theta)$, is close to zero on smooth areas. Notice that this last quantity simply measures the disparity between the angles that $\vec{v}_1$ and the unit normal form with a fixed axis. By the former considerations, any non-decreasing function of $\sin(\psi - \theta)$ with $g(0) = 0$ and $g(1) = 1$ will serve as stopping term. For numerical stability reasons, we compute the eigenvector of maximum eigenvalue in terms of the coefficients of J_ρ. If the tensor J_ρ equals:

$$\begin{pmatrix} G_\rho * \cos^2(\theta) & G_\rho * \cos(\theta)\sin(\theta) \\ G_\rho * \cos(\theta)\sin(\theta) & G_\rho * \sin^2(\theta) \end{pmatrix} = \begin{pmatrix} a_{11}(u) & a_{12}(u) \\ a_{12}(u) & a_{22}(u) \end{pmatrix}$$

Then the tangent of twice the angle, 2ψ, is given by:

$$\begin{aligned} A = A(\theta(u), u) &:= \tan 2\psi = \frac{\sin(2\psi)}{\cos(2\psi)} = \frac{2a_{12}}{a_{11} - a_{22}} \\ &= \frac{2G_\rho * \cos(\theta)\sin(\theta)}{G_\rho * \cos^2(\theta) - G_\rho * \sin^2(\theta)} = \frac{G_\rho * \sin(2\theta)}{G_\rho * \cos(2\theta)} \end{aligned} \tag{7}$$

Noting the vector product with an $\times$, the measure of irregularity, we propose, is as follows:

$$\begin{aligned} g(\theta(u), u) &= \|v_1 \times \vec{n}\|^2 = \sin^2(0.5 \arctan(A) - \theta) \\ &= \sin^2(\psi - \theta) \end{aligned} \tag{8}$$

First notice that the discrete numeric implementation of a convolution with a gaussian is approximated by means of a windowed (squared) kernel or mask. This implies that discrete gaussians are functions of compact support. Second, even in the continuous domain, gaussian kernels are approximations of the identity for the convolution product. That is they converge to the dirac delta as the variance tends to zero. For this (among others) reason they are commonly used in the area of Fourier analysis as a tool to study the "local" behavior of functions [5, 16]. Based on the above considerations, we will refer to the Roughness Measure as local measure of irregularity, in spite of being just an approximation to the local behavior of a function in

the continuous domain. These are the main properties of g:

3.1. *Properties of the Roughness Measure*

This section is devoted to the analysis of those points that cancel the roughness measure. We will prove that g measures the degree of symmetry of the curve around each point and, thus, it cancels on circles. This property is essential for the convergence of RCF to a non trivial steady state. Now, the function g cancels if and only if $\psi - \theta = 0$, which is nothing but the angle of v_1 with respect to the unit normal at each point. This fact motivates, for the sake of notational simplicity, using 'gauge' coordinates, $\vec{t}(u_0)$, $\vec{n}(u_0)$, in order to determine what characterizes those points $\gamma(u_0)$ such that $g(\theta(u_0), u_0) = 0$. By taking angles with respect the axis given by $\vec{n}(u_0)$, the roughness measure equals $\sin^2(\arctan(A))$. Thus if one is to prove that g cancels in symmetric situations it suffices to check that the quantity A computed with respect to $\vec{n}(u_0)$ cancels.

Proposition 3.1. *If the angle of the tangent does not turn more that $\pi/2$, the function g measures the degree of symmetry of the curve around each point.*

Proof: Using 'gauge' coordinates, it suffices to check that $A(u_0) = 0$. We assert that the latter equality is satisfied if and only if $a_{12}(u_0) = 0$. This follows because, by hypothesis, θ does not turn more that $\pi/2$ and we can assure that $a_{11} - a_{22} = \int_{-\infty}^{\infty} G_\rho(u)\cos(2\theta(u)) \neq 0$. If we further take $u_0 = 0$, the coefficient a_{12} equals:

$$\begin{aligned} a_{12}(0) &= \frac{1}{2}\int_{-\infty}^{\infty} G_\rho(u)\sin(2\theta(u))\,du \\ &= \frac{1}{2}\int_{-\infty}^{0} G_\rho(u)\sin(2\theta(u))\,du \\ &\quad + \frac{1}{2}\int_{0}^{\infty} G_\rho(u)\sin(2\theta(u))\,du \end{aligned}$$

By changing the integration variable of the second integral by $-u$, we obtain:

$$\begin{aligned} a_{12}(0) &= \frac{1}{2}\int_{-\infty}^{0} G_\rho(u)\sin(2\theta(u))\,du \\ &\quad + \frac{1}{2}\int_{-\infty}^{0} G_\rho(-u)\sin(2\theta(-u))\,du \end{aligned}$$

Now, by assumption, the curve is symmetric around zero (i.e. $\theta(-u) = -\theta(u)$), so that by symmetry of the gaussian we obtain:

$$\begin{aligned} a_{12}(0) &= \frac{1}{2}\int_{-\infty}^{0} G_\rho(u)\sin(2\theta(u))\,du \\ &\quad - \frac{1}{2}\int_{-\infty}^{0} G_\rho(u)\sin(2\theta(u))\,du = 0 \end{aligned}$$

□

In the discrete version of RCF, since gaussian kernels are of compact support, the above result implies that g measures the local degree of symmetry in a curve. That is, for a given scale ρ, it cancels at those points, $u = u_0$ where the curve is symmetric in a neighborhood of length $2\rho + 1$ centered at u_0. The former Proposition and symmetry of circles yields:

Corollary 3.1. *At whatever scale, ρ, the function* (8) *cancels on circles.*

4. Formulation for the Regularized Curvature Flow (RCF)

For a fixed parameter u of a curve, γ_0, embedded in the plane, we define:

Definition 4.1 (The regularized curvature flow). We suggest is the geometric flow given by:

$$\begin{aligned} \gamma_t &= g(\theta(u), u)\kappa\vec{n} \quad \text{with initial condition} \\ \gamma(u, 0) &= \gamma_0(u) \end{aligned} \tag{9}$$

with the function g given by formula (8), κ denoting the curve curvature and θ the angle of the unit tangent with a fixed axis.

When we consider a parameter change, $u = u(\tilde{u})$, the function g will be assumed to be computed over the convolution given by $\int G_\rho(u)F(u)\,du = \int G_\rho(\tilde{u})F(\tilde{u})u_{\tilde{u}}d\tilde{u}$. Since a curve in the plane is determined by its curvature, by means of the properties of the PDE associated to κ and θ we can infer properties of the family of curves solving (9). Missing proofs in the next pages can be found in the Appendix at the end of the paper.

4.1. Existence of Solutions

Proposition 4.1. *The curvature of the solution to* (9) *parameterized by the angle* θ *satisfies*:

$$\kappa_T = g\kappa + \partial_{\theta\theta}(g\kappa)$$

for a new time T *given by* $\frac{dT}{d\tau} = \kappa^2$.

Notice that the angle is a proper parameter if and only if $\theta_u \neq 0$, hence the above Proposition only makes sense if the curve is convex or between two consecutive inflexion points. Further it ensures, by boot-strap arguments on PDE's [7], existence and uniqueness of solutions for convex curves, as long as the total gaussian curvature remains bounded.

Proposition 4.2. *Let* $\theta_0(s,t)$ *be the angle between the tangent to the initial curve* $\gamma_0(s,t)$ *and a fixed axis. Then the problem given by (9) is equivalent to*:

$$\theta_\tau(s,\tau) = \partial_s(g\theta_s) + \left(\int_0^s g\theta_s^2 ds\right)\theta_s \qquad (10)$$

with initial condition $\theta(s,0) = \theta_0(s)$ *and periodic boundary conditions* $\theta(0,\tau) = \theta(L,\tau)$

As in the case of the mean curvature flow, a weak solution to (10) exists as long as the curvature remains bounded in L^2.

Theorem 4.1. *For any* $\mathcal{C}^2$ *periodic function* $\theta_0(s)$, *there exists a unique periodic weak solution to*:

$$\theta_\tau(s,\tau) = \partial_s(g\theta_s) + \left(\int_0^s g\theta_s^2 ds\right)\theta_s \quad \textit{with}$$
$$\theta(s,0) = \theta_0(s)$$

The solution to (10) is, at least, as differentiable as the initial angular function [9]. Hence RCF has a unique $\mathcal{C}^k$ solution.

4.2. Properties of RCF

Let us enumerate those properties of RCF that are relevant to image filtering. We will distinguish between those ensuring simplification of shapes and the ones describing the asymptotic behavior.

A. Shape Simplification.

Lemma 4.1. *Let* $\kappa(\theta,t)$, $t \in [0,T)$, *be the solution to* (10) *with initial condition* $\kappa_0(\theta)$ *and assume that* $g_{\theta\theta}$ *is bounded by a constant* M. *Then, the following inequality holds*:

$$\max_{0<t<T} |\kappa(\theta,t)| \leq e^{T(M+1)} \max|\kappa_0|$$

Proof: The function $v = e^{-(M+1)t}\kappa$ fulfills the PDE:

$$v_t = -(M+1)v + e^{-(M+1)t}\kappa_t = -(M+1)v + gv + \partial_{\theta\theta}(gv)$$

If the function v had an interior extremum at the set where κ is positive, then:

$$0 = (g - (M+1) + g_{\theta\theta})v + g\partial_{\theta\theta}(v) \leq g\partial_{\theta\theta}(v)$$

Since $g \geq 0$, we get that the extremum is, indeed, a minimum. A similar argument at points with negative κ, yields that $|v(\theta,t)| \leq \max|v(\theta,0)| = \max|\kappa_0|$. We conclude that $|\kappa| \leq e^{(M+1)t}|v|$ and, thus, $\max_{0\leq t<T} |\kappa| \leq e^{(M+1)T} \max_{0\leq t<T}|v| = e^{(M+1)T}\max|\kappa_0|$. □

Proposition 4.3. *The number of inflexion points* (*i.e. zeros of the curvature*) *of a family of curves,* $\gamma(u,t)$, *satisfying* (9) *for* $t \in [0,T)$ *is a non-increasing function of time.*

Proof: We will prove that between two consecutive inflexion points the curvature does not change its sign. In an arc joining two consecutive inflexion points Lemma 4.1 holds and, so, we have that:

$$e^{T(M+1)} \min\kappa_0 \leq \kappa \leq e^{T(M+1)} \max\kappa_0$$

It follows that κ keeps the sign of κ_0 between consecutive inflexion points. □

Proposition 4.4. *Let* $\gamma(u,t)$ *be a family of curves solving* (9), *for* $(u,t) \in [0,1] \times [0,T)$. *Then the energy of the curvature* $\|\kappa(t)\|_{L^2} := \int_0^1 \kappa^2\sqrt{\dot{x}^2 + \dot{y}^2}du = \int_0^1 \kappa^2 v du$ *is a decreasing function of time*,

$$\|\kappa(t)\|_{L^2} \leq \|\kappa(0)\|_{L^2}$$

Remarks.

1. It can be proved that the length, $L(t)$, of a curve satisfying (9) decreases in time at the rate $L_t =$

$-\int g\kappa^2 v du$. It follows that the total curvature also decreases in time:

$$\bar{\kappa}(t) = \int |\kappa|\sqrt{\dot{x}^2 + \dot{y}^2}du \leq L(t)\|\kappa(t)\|_{L^2} \leq L(0)\|\kappa(t)\|_{L^2}$$

which is one of the requirements for curve simplification.

2. The above Proposition ensures existence of weak solutions of the curvature equation for all time, hence we can assure that $\mathcal{C}^\infty$ piece-wise curves exist for all time.

B. Convergence to Smooth Non-trivial Curves. Solutions to the RCF tend asymptotically to a $\mathcal{C}^\infty$ curve, which is the fixed point of Eq. (9) given by $g \equiv 0$. We can summarize this asymptotic behavior in the following results:

Proposition 4.5. *Steady states of* (9) *are simple closed curves.*

Proof: First notice that existence of a Lyapunov functional (the length functional, for instance) ensures that RCF has not periodic orbits. It follows that the limit of any orbit $\gamma(u, t)$ must be a steady point of Eq. (9). The inclusion principle [10] and stability of circles for RCF yield the statement as follows. Let C_1 be a circle containing γ_0 and C_2 a circle included in γ_0. By the inclusion principle, we have that evolutions of these curves under RCF fulfill $C_2(u, t) \subset \gamma(u, t) \subset C_1(u, t)$. The fact that any circle is a steady point yields the result. □

Theorem 4.2. *The roughness measure g tends to zero over the solutions to RCF.*

Proof: See Appendix B for a detailed proof. □

The above Theorem constitutes the main property of RCF, since, on one hand, it ensures that the orbits of RCF converge to a curve conforming to our criterion of regularity. It, further, provides the method with a stop criterion in terms of the magnitude of g which proves to be extremely efficient in practical applications because it stabilizes curves preserving (see Section 5) enough extreme of curvature as to identify the original noisy shapes.

4.3. Numeric Implementation via Level Sets Formulation

The level sets implicit formulation of RCF is given by:

$$u_t = g\left(\frac{\nabla u}{|\nabla u|}\right)|\nabla u|\,\mathrm{div}\left(\frac{\nabla u}{|\nabla u|}\right) \tag{11}$$

The exact implementation would imply tracking, for each image pixel, the level curve though it in order to perform the convolution with a one dimensional gaussian kernel along the level-line. Since this is computationally unfeasible we propose an approximate algorithm, which consists in computing the roughness measure using a gaussian in two variables, $G_\rho(x, y) = \frac{1}{2\pi\rho^2}e^{-(x^2/2\rho^2)-(y^2/2\rho^2)}$. That is, the structure tensor is computed by means of the formula:

$$\tilde{J}_\rho(\vec{n}) = \tilde{J}_\rho\left(\frac{\nabla u}{|\nabla u|}\right) = \int G_\rho(\tilde{x} - x, \tilde{y} - y) \cdot \left[\left(\frac{\nabla u}{|\nabla u|}\right) \otimes \left(\frac{\nabla u}{|\nabla u|}\right)\right] d\tilde{x}d\tilde{y}$$

We assert that if $u(x, y, 0)$ is the signed distance map, d, to the initial curve, then $\tilde{J}_\rho$ approximates J_ρ locally. For the sake of notational simplicity the scale ρ will be dropped, the projection matrix onto a vector v will be noted by P_v and convolutions will be evaluated at the origin.

Firstly, we have that, in the case of evolving the signed distance map, it exists a neighborhood of γ_0 given by $\Omega = \{(x, y)\,;\, |d(x, y)| < \epsilon\}$, such that the curves of level $|\delta| \leq \epsilon$ are:

$$\gamma_\delta(u) = \gamma_0(u) + \delta\vec{n}_0(u)$$

This follows by existence of tubular neighborhoods. Since the curve γ_0 is diffeomorphic to the unit circle (i.e. a compact manifold with trivial normal bundle), a tubular neighborhood [22] of size ϵ exists. Besides it can be parameterized by:

$$[a, b] \times [-\epsilon, \epsilon] \to \Omega \subset \mathbb{R}^2$$
$$(u, \delta) \mapsto \gamma_0(u) + \delta\vec{n}_0(u)$$

Hence, in the parameter space of the tube (Fig. 1(c)), the normal vectors, $\vec{n}(u, \delta)$, coincide with $\vec{n}_0$, that is, $\vec{n}(u, \delta) = \vec{n}(u) = \vec{n}_0(u)$, $\forall\delta \in (-\epsilon, \epsilon)$. In the image domain, this coincidence corresponds to equal normal vector for the level curves in Ω when we move in the

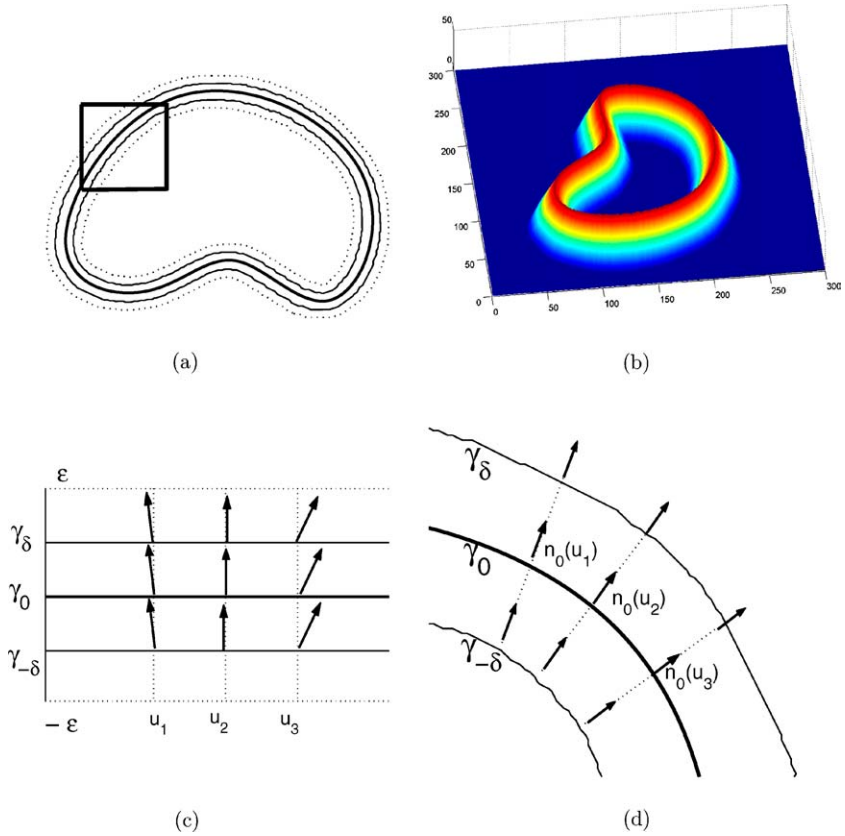

Figure 1. Tubular neighborhood in the image domain (a), narrow band (b) and normal vectors in the tube parameter space (c) and in the image domain (d).

normal direction to γ_0 (see the drawings in Fig. 1(a) and (d)). The curves of Fig. 1(a) are level curves of the signed distance map to the bold face curve inside a tube represented by the dotted boundary curves. Coincidence of normal vectors for the level curves inside the square is illustrated in Fig. 1(d).

By the above considerations, we conclude that if we computed our approximation $\tilde{J}$ in the parameter space of the tube it would be proportional to the exact J:

$$\tilde{J} = G(u,\delta) * P_n(u,\delta) = \int_{-\epsilon}^{\epsilon}\int_{-\infty}^{\infty} e^{-\frac{u^2}{\rho^2}} e^{-\frac{\delta^2}{\rho^2}} \cdot P_n(u)\,du d\delta = \int_{-\epsilon}^{\epsilon} e^{-\frac{\delta^2}{\rho^2}} d\delta \int_{-\infty}^{\infty} e^{-\frac{u^2}{\rho^2}} \cdot P_{n_0}(u)\,du = K \cdot J$$

It follows that the roughness measure computed over $\tilde{J}$ equals the true g. When we, instead, convolve in the image domain, $\tilde{J}$ splits into the integrals:

$$\tilde{J} = \int_{\Omega} G \cdot P_{n_0}\,dx\,dy + \int_{\Omega^c} G \cdot P_n\,dx\,dy = I_{\Omega} + I_{\Omega^c}$$

The first integral approaches the convolution in the parameter space (u,δ), meanwhile the magnitude of the second is as tiny as the remains of the two dimensional gaussian. The latter error vanishes if one uses a narrow band strictly included in the tube. That is, by forcing the function u representing the curve evolution to be constant outside the tube. Notice that this is equivalent to considering that $\tilde{J}$ solves the heat equation for initial condition $P_n \cdot \chi_{\text{Band}}$, where χ_{Band} denotes the characteristic function of the narrow band. From now on, we will assume that $P_n = P_n \cdot \chi_{\text{Band}}$. The mesh shown in Fig. 1(b) corresponding to the absolute value of the signed distance map to the bold face curve in Fig. 1(a) is an example of the way a narrow band works. We notice the reader that in the discrete numeric implementation, no band is needed, since a

discrete gaussian is of compact support. The only requirement that is to be satisfied is that, for each point of γ_0, the support of the discrete gaussian is included in the tube. This gives a bound on the maximum scale ρ supported by the discrete level sets formulation in terms of the initial curve.

It only remains to derive a formula for the error introduced by the coordinate change in the tube. In a level sets formulation, the parameter of a curve is the implicit one, namely the one given by the x-coordinate. We notice that, although the latter is a local parameter and, so, the formula we are about to give only applies to bounded domains of integration, K, there is no loss of generality as this is the case in the numeric implementation. Hence, let us assume that the curves γ_δ are implicitly given by $\gamma_\delta^{Im}(x) = (x, y_\delta(x))$, in particular the tubular coordinates are determined by the implicit parameter of $\gamma_0 = (x, y_0(x))$. Now, the integral I_K would yield the exact value of $J|_{\Phi^{-1}(K)}$ if for a fixed $x = x_0$, the implicit parameterization γ_δ^{Im} was equal to the tubular one, as in this case, we would have:

$$\begin{aligned} e^{-x_0^2} P_n(x_0, y) &= e^{-x_0^2} P_n(x_0, y_\delta(x_0)) \\ &= e^{-x_0^2} P_n(\Phi(x_0, \delta)) = e^{-x_0^2} P_n(\Phi(x_0, 0)) \\ &= e^{-x_0^2} P_n(x_0, y_0(x_0)) \end{aligned}$$

so that integrating over the domain $K = [-a, a] \times \mathbb{R}$ supporting the implicit parameter:

$$\begin{aligned} &\int e^{-y^2} \int_{-a}^{a} e^{-x^2} P_n(x, y)\, dx\, dy \\ &\quad = \int e^{-y^2} \int_{-a}^{a} e^{-x^2} P_{n_0}(x, y_0(x))\, dx\, dy \\ &\quad = \int e^{-y^2} \int_{-a}^{a} e^{-x^2} P_{n_0}(x)\, dx\, dy \end{aligned}$$

Unfortunately this is not the case, in general, as the polygonal curve of Fig. 2 illustrates. The implicit parameterization corresponds to cuts of the curves γ_δ with the horizontal lines, meanwhile the parameterization induced by the tube is given by the cuts with the normal lines to γ_0. It follows that $e^{-x_0^2}$ does not weight the matrix $P_n(\Phi(x_0, \delta))$, but the matrix corresponding to a point $\bar{x}_0$ obtained by projecting onto γ_0 the point $(x_0, y_\delta(x_0))$ along its normal direction (Fig. 2(a)). This implies that $e^{-x^2} P_n(x, y) = e^{-x^2} P_n(x, y_\delta(x)) = e^{-x^2} P_n(\bar{x}, y_0(\bar{x})) = e^{-x^2} P_n(\bar{x})$. The explicit change of coordinates in γ_0 that makes values match (see Fig. 2(b) for a graphical representation) is derived using trigonometric arguments:

$$\begin{aligned} \bar{x} = x + \delta \sin(\theta(\bar{x})) \Rightarrow \bar{x} &= x + \delta(\sin(\theta(x)) \\ &+ \cos(\theta(x))\theta_x(x)(x - \bar{x}) + \mathcal{O}((x - \bar{x})^2) \end{aligned}$$

Since $|x - \bar{x}| = \delta \sin(\theta(\bar{x})) = \mathcal{O}(\delta)$, it follows that the change of coordinates $\bar{x}$ is given by:

$$\bar{x} = x + \delta \sin(\theta(x)) + \mathcal{O}(\delta^2)$$

Finally the Taylor development of $P_{n_0}(\bar{x}) = P_{n_0}(x + \delta \sin(\theta(x)) + \mathcal{O}(\delta^2))$ yields that $\tilde{J}$ equals:

$$\begin{aligned} \tilde{J} = &\int e^{-y^2} \int e^{-x^2} P_{n_0}(x)\, dx\, dy \\ &+ \int e^{-y^2} \int e^{-x^2} \delta \sin(\theta(x)) \partial_x(P_{n_0})\, dx\, dy \\ &+ \mathcal{O}(\delta^2) = C \cdot J|_{\Phi^{-1}(K)} + Error \end{aligned}$$

It is not difficult to check that the error introduced does not alter the essential properties of the roughness measure given in Section 3. Furthermore, we notice that

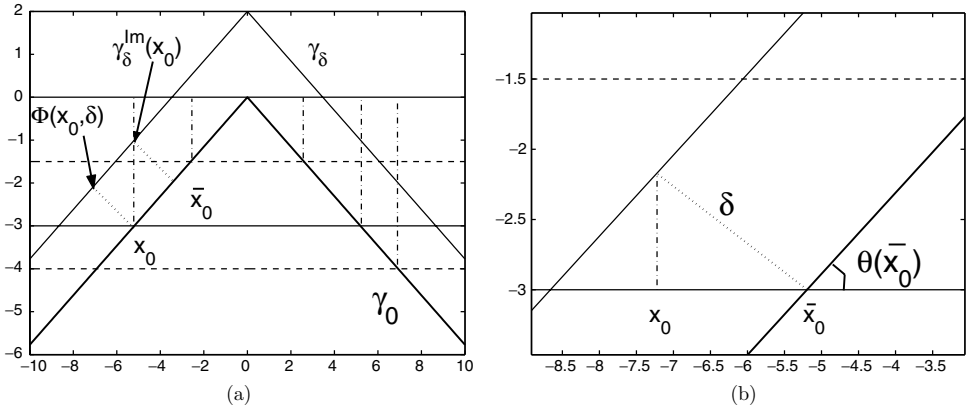

Figure 2. Tube parameterization versus implicit (a) and coordinate change (b).

in a discrete implementation, curves are polygonal so that the error introduced is nearly zero (as $\partial_x(P_{n_0}) \equiv 0$ except at junctions).

Notice that images with irregular level curves on a textured or noisy background may evolve so that motion of level curves does not agree with RCF. The roughness measure could cancel on the regular curve but not in the noisy neighborhood. However, other curvature based techniques, successfully used in image processing present a similar pathology. The min/max flow [14], for instance, bases motion on the image average around each point. Moreover our numerical experiments show that the dependency upon the embedding function does not affect the final shapes achieved with RCF.

5. Numerical Experiments

Two different kinds of experiments are presented:

- Tests on synthetic curves with regular and irregular shapes in order to determine the asymptotic behavior of the different geometric flows.
- Tests on noisy and real images illustrating the robustness of the numeric approximation of Section 4.3 against different embedding functions as well as its applicability in practical situations.

5.1. Tests on Synthetic Shapes

This first experiment is designed to assess the asymptotic behavior and properties of RCF and to compare it to the geometric flows of Section 2, Mean Curvature Flow (MCF) and Min/Max Flow (MMF). All techniques are implemented using a finite difference Euler scheme for their level sets formulations. Images showing distance maps plot negative values in black and positive ones in white. Noise removal capabilities will be checked by running the algorithms on a corrupted version of a set of test curves. The graphics of the speeds of the evolutions, as well as the roughness measure g are illustrative of the asymptotic behavior of each of the flows. We assume evolutions have reached their steady states when either speeds are under a given epsilon (criterion A) or they stabilize (criterion B). In the particular case of RCF, by Theorem 6.2, we take the roughness measure as speed of the evolution.

Figure 3 shows the set of test shapes used to analyze the asymptotic behavior of the different flows. The result of applying the different geometric flows

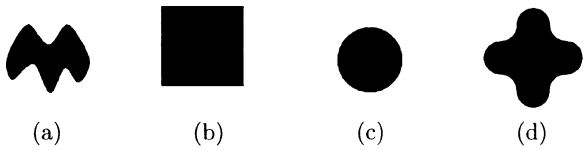

Figure 3. Synthetic shapes of test: (a) M-shape, (b) square, (c) circle and (d) petal.

are shown in Fig. 4 for the case of the circle and the square and in Fig. 5 for the petal and M-shape. Circles and squares (Fig. 4(a) and (d)) are, as the theory stated, steady curves of RCF. Furthermore, any initial curve tends asymptotically towards a steady curve that keeps the same number of inflexion points and curvature extreme than the original shape (petal and M-shape in Fig. 5(a) and (d)). Evolution under MMF stabilizes polygonal curves (square in Fig. 4(e)), prone to significantly differ from the original curve (circles in Fig. 4(b) and M-shape in Fig. 5(e)). In fact, we have observed that MMF tends to produce convex polygonal curves, as the evolution of the M-shape in Fig. 5(e) illustrates. In the case of MCF, a stop criterion based exclusively on the magnitude of the curvature makes shapes reach their trivial steady state. Besides, although MCF speed (Fig. 7(b)) is the smoothest one, stop criterion B stabilizes the evolution at curves (the ones shown in Fig. 4(c) and (f) and Fig. 5(c) and (f)) that hardly keep relevant geometric features from the original shapes. This is due to the fact that evolution under MCF converges rapidly to the convex (round in the limit) final state as the M-shape, the petal (Fig. 5(c) and (f)) and the square (Fig. 4(c)) illustrate.

Our tests on noisy curves show that all methods have similar noise removal properties and only differ in the final shape obtained, which depends on the asymptotic behavior of the underlying shape. Since MCF converges to trivial states, only results for RCF and MMF are displayed. The shapes recovered with RCF are the ones shown in Fig. 6(b) and (e). Notice that they are the only ones that produce a smooth curve capturing the essential geometry of the original free noise shape. In fact, the final curves obtained do not significantly differ from the steady states of the noisy free shapes of Figs. 4 and 5. Evolution under MMF failed to stabilize for any of the two stop criteria, essentially by the highly oscillating nature of the evolution speed (plot in Fig. 7(b)). Images shown in Fig. 6(c) and (f) were obtained after 3000 iterations. Comparing with RCF we observed that the model of the shapes that MMF recovers is worst, especially in the case of the circle (Fig. 6(c)), where it restores a square.

Figure 4. Asymptotic Behavior of circle and square: RCF steady states (a), (d), images obtained with MMF (7500 iterations) (b) and (e) and stabilization of MCF (c) and (f).

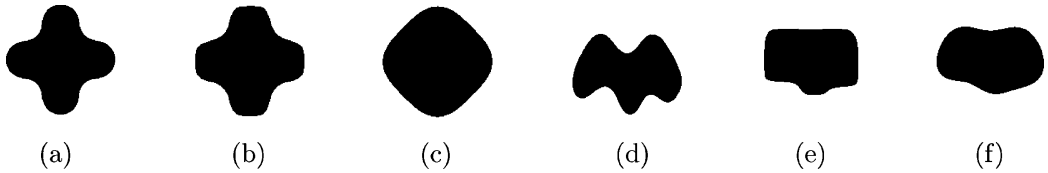

Figure 5. Asymptotic Behavior of petal and M-shape: RCF steady states (a) and (d), images obtained with MMF (7500 iterations) (b) and (e) and stabilization of MCF (c) and (f).

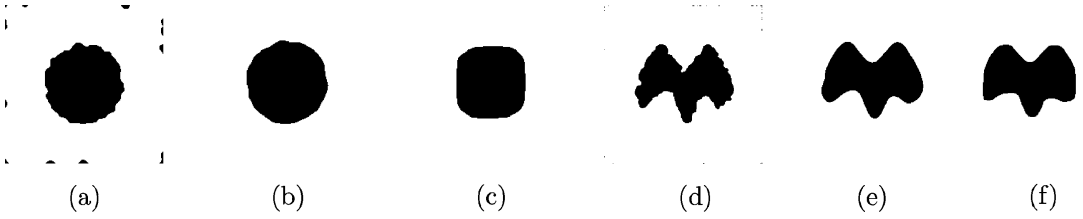

Figure 6. Irregular curves, circle (a) and M-shape (d). RCF smoothing of circle (b) and the M-shape (e) and MMF (3000 iterations) over circle (c) and the M-shape (f).

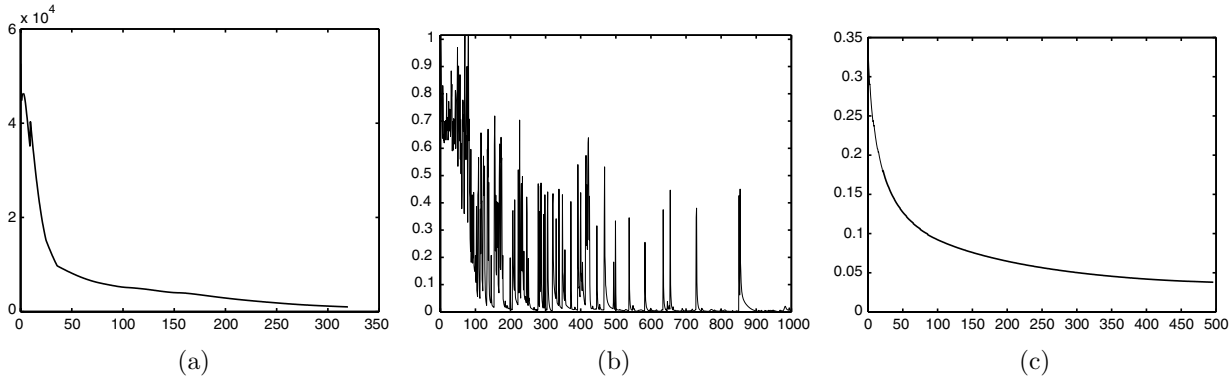

Figure 7. Graphics for the roughness measure, (a) and speeds for MMF (b) and MCF (c).

Graphics for the roughness measure (Fig. 7(a)) illustrate that not only does g decrease in time (Theorem 6.2) but also that it tends asymptotically to zero. This motivates choosing stabilization of the roughness measure as the stop criterion when we deal with highly noisy images. We also notice the reader the irregular plot of MMF speed (Fig. 7(b)), since it reflects the limited efficiency of the method for practical applications. A stop criterion in terms of speed stabilization fails to stabilize evolutions under MMF and only by fixing the number of iterations it is possible to restore shapes. Finally, although the graphic for MCF (Fig. 7(c)) is the smoothest one, rapid convergence to a convex curve, makes any stop criterion useless to shape restoration.

5.2. Tests on Real Images

This part is devoted to results on real images obtained with RCF. We first present a comparison

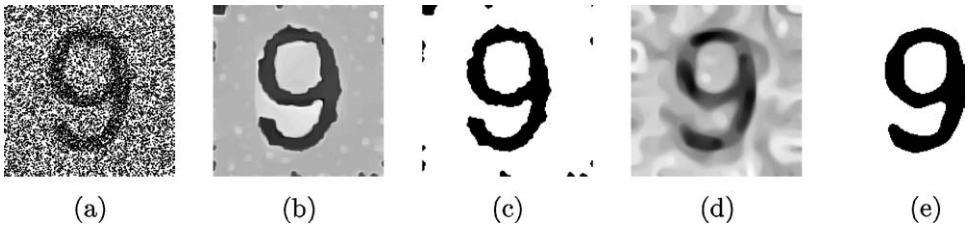

Figure 8. Noisy numbers. Noisy number (a), smoothing with MMF (b), reconstruction with MMF (c), smoothing with RCF (d) and restoration (e).

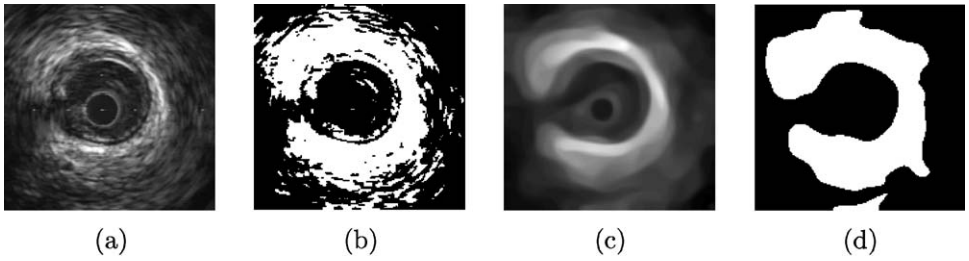

Figure 9. Cross Sections of IVUS sequences. Original IVUS images (a) and segmenting surface (b), steady state attained with RCF (c) and the resulting segmenting surface (d).

to images filtered with MMF in order to illustrate the better quality of the shapes recovered. We also show medical images filtered with RCF that show the efficiency of RCF in practical situations.

5.3. Noisy Numbers

We have used our method to reconstruct numbers extracted from real noisy images. Reconstructions result from applying a threshold of 0.5 to the filtered images. In Fig. 8, we can find the reconstructions of a noisy nine (Fig. 8(a)) obtained with MMF (Fig. 8(c)) and RCF (Fig. 8(f)). The smoothed images of Fig. 8(b) and (e) are the steady states attained by MMF and RCF, respectively. Both techniques succeeded in removing noise from the original image and recovering a number that can be identified as a nine. Although the filtered image obtained with MMF presents a better visual quality than the one produced by RCF, the model of the number extracted from the image that RCF yields is, clearly, smoother than the representation obtained with MMF. Notice also that images filtered with MMF present small black artifacts near their boundaries.

5.4. Application to Medical Images Smoothing

We have applied our technique to segment the luminal area in intravascular ultrasound sequences (IVUS). Since the grey level of ultrasound images expresses the material impedance, black pixels correspond to blood and white ones to tissue. The aim was to obtain a model of the artery reflecting its geometry by means of a procedure requiring the minimal manual intervention as possible. Artifacts caused by blood flow and the speckled nature of ultrasound images force some kind of smoothing of the level surfaces.

The technique proposed has been applied to cross sections and longitudinal cuts. Figure 9(a) shows a cross section and Fig. 9(b) the level surface segmenting blood from tissue. The inner border of the largest white shape is the curve segmenting blood and tissue. Isolated white areas in the interior of the black circle are product of noise. The image achieved by RCF is displayed in Fig. 9(c) and the corresponding segmenting surface in Fig. 9(d). Notice that small artifacts have been removed while the segmenting curve is preserved. In Fig. 10 we find a longitudinal section (Fig. 10(a)) and the segmenting curve (Fig. 10(c)). The wavy shape, characteristic of IVUS longitudinal cuts, reflects cardiac motion and is of clinical interest. Smoothed

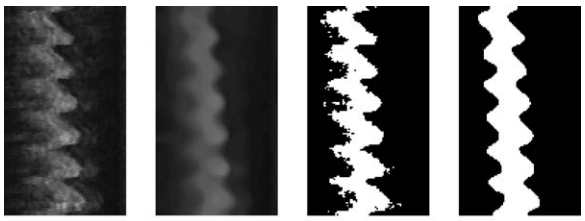

Figure 10. Longitudinal cut of IVUS (a), images smoothed with RCF (b). Shape segmenting blood and tissue in (c) the original cut and RCF (d).

versions using RCF and the resulting segmenting level surfaces are shown in Fig. 10(b) and (d), respectively. Notice that RCF recovered a smooth shape keeping the same number of undulations than the original cut.

6. Conclusions

In the present paper, we have developed the theoretical background for a method focused on obtaining a geometric flow guaranteing convergence to non trivial smooth curves. Our numerical experiments show its ability to restore smooth models of the level curves in noisy images.

Based on the former limitations and advantages of each of the actual filtering techniques, we have developed an image filtering operator that benefits from the smoothing effects of mean curvature flow limiting its trivialization of shapes. The key point of the proposed technique is the introduction of a local measure of curve smoothness dependent on the curvature variation along the level set curves, rather than on the magnitude of the curvature or image intensity. We show that this roughness measure is useful to define a stopping term in a curvature flow. Furthermore, the fact that the measure of irregularity decreases on the orbits of the flow, provides us with a stopping criterion that produces a smooth steady state keeping enough significant characteristics as to identify the original shape. The results obtained on synthetic shapes, point out that the RCF succeeds in recovering a smoothed version of the original curve that keeps significant inflexion points and curvature extreme. Hence, it makes a later recognition of shapes easier. Experiments performed on real images illustrate its efficiency in practical applications.

Appendix A: Existence of Solutions to RCF

Proposition 6.1. *The curvature of the solution to* (9) *parameterized by the angle θ satisfies*:

$$\kappa_T = g\kappa + \partial_{\theta\theta} g\kappa \quad with \quad \frac{dT}{d\tau} = \kappa^2$$

Proof: The change to the angular parameter induces a coordinate change in the domain of definition of the equation, $(u, t) \mapsto (\theta(u, t), \tau(t))$, given by the partial derivatives $\partial_u = \theta_u \partial_\theta$ and $\partial_t = \theta_t \partial_\theta + \tau_t \partial_\tau$. Now, following [8, 10], we have that the angle, θ, and the curvature satisfy:

$$\theta_t(u, t) = \partial_s(g\kappa) \quad \text{and} \quad \kappa_t(u, t) = g\kappa^3 + \partial_{ss}(g\kappa)$$

Since, without loss of generality we can take $\tau_t = 1$, differentiating with respect to the new time variable, we have that the curvature fulfills:

$$\kappa_\tau = -\theta_t \kappa_\theta + \kappa_t = -\kappa_\theta \partial_s(g\kappa) + g\kappa^3 + \partial_{ss}(g\kappa)$$

Using the relation between partial derivatives $\partial_s = \kappa \partial_\theta$, we get that:

$$\kappa_\tau = g\kappa^3 + \kappa^3 \partial_{\theta\theta}(g\kappa)$$

Finally, consider a new time derivative, dT defined by $\frac{dT}{d\tau} = \kappa^2$ to obtain:

$$\kappa_T = \partial_T(\kappa(\theta, t(T))) = \kappa_t \frac{dt}{dT} = g\kappa + \partial_{\theta\theta}(g\kappa)$$

□

Proposition 6.2. *Let $\theta_0(s, t)$ be the angle between the tangent to the initial curve $\gamma_0(s, t)$ and a fixed axis. Then the problem given by* (9) *is equivalent to*:

$$\theta_\tau(s, \tau) = \partial_s(g\theta_s) + \left(\int_0^s g\theta_s^2 \, ds \right) \theta_s \qquad (12)$$

with initial condition $\theta(s, 0) = \theta_0(s)$ and periodic boundary conditions $\theta(0, \tau) = \theta(L, \tau)$.

Proof: In the case of the arc-length parameter and also taking $\tau_t = 1$, the coordinate change [8, 10] in the domain of definition of the solutions to (9) is given by $\partial_u = \|\gamma_u\| \partial_s$ and $\partial_t = -(\int_0^s g\theta_s^2 ds)\partial_s + \partial_\tau$ Therefore,

we have that:

$$\theta_\tau(s,\tau) = \theta_t + \left(\int_0^s g\theta_s^2 ds\right)\theta_s = \partial_s(g\theta_s) + \left(\int_0^s g\theta_s^2 ds\right)\theta_s$$

where the last equality follows from the expression of θ_t ([8, 10]). This yields that angles of solutions to (9) satisfy (12). Conversely, for any solution to (12) the curves:

$$\gamma(s,t) = \left(\int_0^s \cos(\theta)\, d\tilde{s}, \int_0^s \sin(\theta)\, d\tilde{s}\right)$$

are closed curves that satisfy an equation that, up to a change of parameter, equals (9). □

For the next theorem, we give a sketch of proof and refer the reader to [6] for further details.

Theorem 6.1. *For any $\mathcal{C}^2$ periodic function $\theta_0(s)$, there exists a unique periodic weak solution to*:

$$\theta_\tau(s,\tau) = \partial_s(g\theta_s) + \left(\int_0^s g\theta_s^2 ds\right)\theta_s \quad \textit{with}$$
$$\theta(s,0) = \theta_0(s)$$

Proof: Let $X = \mathcal{C}([0,T], H^1(I,\mathbb{R}))$ be the space of continuous functions from $[0,T]$ to the Sobolev space of periodic real functions with first derivatives square integrable. Each function, $\psi \in X$, defines the linear parabolic PDE:

$$\theta_t(s,t) = \partial_s(a(s,t)\theta_s) + b(s,t)\theta_s$$
$$\text{with initial condition} \quad \theta(s,0) = \theta_0(s)$$

with $b(s,t) := (\int_0^2 g(\psi)\psi_s^2 ds)$ and $a(s,t) := g(\psi)$. By general theory on parabolic differential equations ([5]), we know that, at least, a $\mathcal{C}^2$ solution satisfying the maximum principle exists. Furthermore, by virtue of the equation associated to its first derivative, $\theta_s = \kappa_s$, we have that

$$\max_{0<t<T} \|\kappa\|L_2 \le e^T \max\|\kappa_0\| \tag{13}$$

Consider the sequence in H^1 defined as:

$$\theta^1 := A(\theta_0); \quad \theta^k := A(\theta^{k-1})\ k > 1$$

We claim that the sequences θ^k and θ_t^k are bounded in $L^2([0,T], H^1(I,\mathbb{R}))$ and $L^2([0,T], H(I,\mathbb{R})^{-1})$, respectively, where $H(I,\mathbb{R})^{-1}$ denotes the topological dual space of $H^1(I,\mathbb{R})$. Then, since the spaces are reflexive, there exists subsequences, θ^{k_m} and $\theta_t^{k_m}$ and a function $\theta \in L^2([0,T], H^1(I,\mathbb{R}))$ with $\theta_t \in L^2([0,T], H(I,\mathbb{R})^{-1})$ such that:

$$\theta^{k_m} \rightharpoonup \theta \text{ weakly in } L^2([0,T], H^1(I,\mathbb{R})) \quad \text{and}$$
$$\theta_t^{k_m} \rightharpoonup \theta_t \text{ weakly in } L^2([0,T], H^1(I,\mathbb{R})^*)$$

This function θ is a weak solution [7] (by virtue of Lipschitzity of g) to the initial boundary problem of Proposition 6.2 and produces a piece wise smooth curve that solves Eq. (9)

The maximum principle for solutions to (12) and the inequality (13), gives a bound for $\|\theta^k\|^2_{L^2([0,I],H^1(I,R)))}$. For a bound on θ_t^k in H^{-1}, consider, for each $\omega \in H^1$, the following:

$$\left|\int \theta_t^k \omega\right| = \left|-\int a(s,t)\theta_s\omega_s + \int b(s,t)\theta_s\omega\right|$$
$$\le \|\theta_s\|_{L^2}\|\omega_s\|_{L^2} + C\|\theta_s\|_{L^2}\|\omega\|_{L^2}$$
$$\le (e^T\|\kappa_0\|_{L^2} + C\|\kappa_0\|_{L^2})\|\omega\|_{H^1}$$

where we have applied Holder to obtain the first inequality. It follows that $\|\theta_t^k)\|_{H^{-1}} \le e^T\|\kappa_0\|_{L^2} + C\|\kappa_0\|_{L^2}$. Weakly convergence for bounded sequences in reflexive spaces yields existence of weak solutions for finite time. Uniqueness can be proved by means of Gronwall's inequality. □

In [9] it is shown that solutions to (6.2) are as differentiable as the initial function. It follows that θ is, at least, a $\mathcal{C}^2$ classic solution.

Appendix B: Properties of RCF

Energy Bounds

Proposition 6.3. *Let $\gamma(u,t)$ be a family of curves solving* (9), *for $(u,t) \in [0,1]\times[0,T)$. Then the energy of the curvature $\|\kappa(t)\|_{L^2} := \int_0^1 \kappa^2\sqrt{\dot{x}^2+\dot{y}^2}du = \int_0^1 \kappa^2 v du$ is a decreasing function of time*,

$$\|\kappa(t)\|_{L^2} \le \|\kappa(0)\|_{L^2}$$

Proof: We will see that the inequality is fulfilled between two consecutive inflexion points, θ_i, θ_{i+1}. Since

κ belongs to the Sobolev space $H_0^1(\mathbb{R})$ of functions with compact supports with first derivatives in L^2, it can be expressed as $\kappa = \sum d_n(t)\omega_n$, where the functions ω_n are the eigenvectors of the Laplacian operator $-\Delta$ and we may assume they are positive. We will prove that the coefficients $d_n(t) = \int_{\theta_i}^{\theta_{i+1}} \omega_n \kappa$ decrease in time. Let η denote d_n for an arbitrary n. If we differentiate with respect to time and integrate by parts, as $\kappa = 0$ at θ_i, θ_{i+1}, by Proposition 6.1, we obtain:

$$\eta_t = \int_{\theta_i}^{\theta_{i+1}} \omega_n \partial_{\theta\theta}(g\kappa)\, d\theta + \int_{\theta_i}^{\theta_{i+1}} \omega_n g\kappa d\theta$$

If $\partial_{\theta\theta}(g\kappa) \neq 0$, integrating again by parts the first integral we get

$$\begin{aligned}\eta_t &= \int_{\theta_i}^{\theta_{i+1}} \partial_{\theta\theta}(\omega_n)(g\kappa) d\theta + \int_{\theta_i}^{\theta_{i+1}} \omega_n g\kappa\, d\theta \\ &= (1-\lambda_n)\int_{\theta_i}^{\theta_{i+1}} \omega_n g\kappa\, d\theta\end{aligned}$$

where $\lambda_n = (n\pi)^2$ are the eigenvalues of the Laplacian operator $-\Delta$. Since $(1-\lambda_n) < 0$ and $\omega_n g\kappa$ is positive, if $\kappa > 0$, and negative otherwise, we have that $\eta_t < 0$ when $\kappa > 0$ and $\eta_t > 0$ when $\kappa < 0$. This fact implies $(\eta(t))$ that decreases in time, which proves the result if $\partial_{\theta\theta}(g\kappa) \neq 0$.

In the case that $\partial_{\theta\theta}(g\kappa) \equiv 0$ we are going to show that either the arc remains steady or we have a circle. In any case, since circles are steady curves we have that $\eta(t) \equiv \eta(0)$. The fact that $\partial_{\theta\theta}(g\kappa) \equiv 0$ implies that $\partial_\theta(g\kappa) = f(t)$. Now, since at the boundary points, we have that $g\kappa(t,\theta_i) = g\kappa(t,\theta_{i+1}) = 0$, there exists an interior extremum, that is the first derivative $\partial_\theta(g\kappa)$ cancels at some point. This implies that, indeed, $\partial_\theta(g\kappa) \equiv 0$ on the whole arc, hence we have that is $g\kappa$ is constant and equal to zero, by virtue of the cancellation of κ at the boundary points. So let us assume that we have a convex curve and check that it necessarily must be a circle. Since in this case $\theta_i = \theta_{i+1}$ the first derivative $\partial_\theta(g\kappa)$ must cancel in the whole curve. Developing the derivative, we obtain that $\frac{-g_\theta}{g} = \frac{\kappa_\theta}{\kappa}$. Integrating this equation, we can write the curvature in the form $\kappa = F(t)e^{1/g}$. Substituting this expression in the PDE for the curvature, we get:

$$\kappa_t = F' e^{\frac{1}{g}} - F\frac{g_t}{g^2} e^{\frac{1}{g}} = gFe^{\frac{1}{g}}$$

Now, because $\theta_t = \partial_s(g\kappa) = \kappa\partial_\theta(g\kappa)$, we have that the derivative with respect to time of the factors of the function A given by (7) cancel:

$$\begin{aligned}\partial_t(a_{12}) &= G_\rho * (2\theta_t \cos(2\theta)) \quad \text{and} \\ \partial_t(a_{11} - a_{22}) &= G_\rho * (2\theta_t \sin(2\theta)))\end{aligned}$$

It follows that $g_t \sim \sin(0.5 * \arctan(A) - \theta)(A_t/(1 + A^2) - \theta_t) = 0$. and $F' e^{\frac{1}{g}} = gFe^{\frac{1}{g}}$. Hence F satisfies the differential equation $\frac{F'}{F} = g$. Finally, since g is independent of time, this last equality implies that, indeed, $g = C_1$ is constant. Thus $\kappa = F(t)e^{\frac{1}{C_1}}$ and the curve is a circle. □

Asymptotic Behavior

Before proceeding to the proof of the main property of RCF concerning convergence to zero of the roughness measure (Theorem 6.2), let us begin with some notations and considerations. The norm of the first derivate of a curve solving (9) will be noted by $\nu = \sqrt{\dot{x}^2 + \dot{y}^2}$. Following [7, 8] it is easy to check that ν solves:

$$\nu_t = -g\kappa^2\nu \quad \text{with initial condition } \nu(u,0) = \nu^0(u)$$

since ν is a decreasing function of time, it is bounded above by ν^0. Furthermore, non trivality of steady states of curves following RCF (Proposition 5) yield that ν is also bounded from below by the minimum, $\nu_{\min} > 0$, of the norms corresponding to the limit curve. Also by Proposition 5, we know that the orbits of (9) converge to a curve fulfilling $g\kappa \equiv 0$. Since the latter quantity is continuous (g is Lipschitz [9]) with respect the L^2-norm, it follows that:

$$\begin{aligned}\int g\kappa^2 = \int g\kappa \cdot \kappa &\leq \|g\kappa\|_{L^2}\|\kappa\|_{L^2} \\ &\leq \|g\kappa\|_{L^2}\|\kappa(s,0)\|_{L^2} \overset{t\to\infty}{\longrightarrow} 0\end{aligned}$$

We will note t_0 a time such that $\int g\kappa^2 < \epsilon$. The lower bound $\nu_{\min}$ and the former asymptotic behavior will be used in the proof of Theorem 6.2. Let us begin with a preliminary Lemma:

Lemma 6.1. *The norm, ν, satisfies*:

$$\max_{t\leq T} |\partial_u(\nu^2)| \leq TM\nu^2(u,0) + \nu_u^2(u,0)$$

Proof: Recall that solutions to (6.2) are $\mathcal{C}^2$ classic solutions that converge to a smooth function $\theta_{\lim}$

by existence of Lyapunov functionals. It follows that $\partial_u(g\kappa^2) \to \partial_u(g_{\lim}\kappa^2_{\lim})$ and, hence, $\partial_u(g\kappa^2)$ is uniformly bounded by a constant $M/2$. Integrating (14) and noting $I = \int g\kappa^2 dt$, we get that $\nu = e^{-I}\nu(u,0)$, so that the first derivative:

$$|\partial_u(\nu^2)| = |-2\nu^2 \int \partial_u(g\kappa^2)dt| + |e^{-2I}\nu_u^2(u,0)| \leq Mt\nu^2(u,0)| + \nu_u^2(u,0)$$

□

Theorem 6.2. *The roughness measure g tends to zero over the solutions to RCF.*

Proof: We recall that one of the definitions of the roughness measure is the square norm of the vector product:

$$g(\theta) = \|\vec{v}_1 \times \vec{n}\|^2$$

where the vector $\vec{v}_1$ $(\cos\psi, \sin\psi)$ is given by the quantity:

$$A := \tan 2\psi = \frac{2a_{12}}{a_{11} - a_{22}} = \frac{G_\rho * \sin(2\theta)}{G_\rho * \cos(2\theta)}$$

Therefore, by the above definition of A, g is close to zero in the measure that the vectors $\vec{v}_1 = \tilde{T}_\rho = (G_\rho * \sin(2\theta), G_\rho * \cos(2\theta))$ and $T = (\sin(2\theta), \cos(2\theta))$ coincide. We will check that in the limit, when t goes to infinity, T converges to $\tilde{T}_\rho$. To such purpose we will study the asymptotic behavior of the PDE's that the former vectors follow.

For a given parameter u for a curve following (9), we have that T solves the PDE:

$$T_t(u,t) = \partial_s(gT_s(u,t)) = \frac{1}{\nu}\partial_u\left(g\frac{T_u}{\nu}\right) \quad \text{with} \quad T(s,0) = T_0 \tag{15}$$

where $\nu = \sqrt{\dot{x}^2 + \dot{y}^2}$. On the other hand, $\tilde{T}_\rho$ corresponds to the solution at time $t = \rho$ of:

$$\tilde{T}_t = \tilde{T}_{uu} \quad \text{with} \quad \tilde{T}(u,0) = T(u,t) \tag{16}$$

If we change to the arc length parameter of $\gamma(u,t)$, the above PDE's convert to:

$$T_t = \partial_s(gT_s) + \left(\int g\kappa^2\right)T_s \quad \text{with} \quad T(s,0) = T_0 \tag{17}$$

$$\tilde{T}_t = \nu\partial_s(\nu\tilde{T}_s) + \left(\int g\kappa^2\right)\tilde{T}_s \quad \text{with} \quad \tilde{T}(s,0) = T(s,t) \tag{18}$$

where $\nu = 1/u_s = \nu(s)$ denotes the derivative of the inverse change from parameter u to parameter s. First, notice that in (18) s does not need to correspond to the arc length of $\tilde{T}$. Second, the quantity $g\kappa^2$ is computed over the solution to RCF wiht the function g given by the parameter u. For a better handling of (18), we will develop the term of the second derivative and use the formulation:

$$\tilde{T}_t = \nu^2\tilde{T}_{ss} + \frac{1}{2}\partial_s(\nu^2)\tilde{T}_s + \left(\int g\kappa^2\right)\tilde{T}_s \tag{19}$$

Let t_0 be a time such that $\int g\kappa^2 < \epsilon$, and consider the solutions to (17), (19) with initial condition $T(s,t_0)$. Let $(T-\tilde{T})^2$ be the square of the norm of the difference vector and define $\eta(t)$ to be:

$$\eta(t) = \int (T-\tilde{T})^2 ds \quad \text{for times } t > t_0 \tag{20}$$

If we note $I_g = \int g\kappa^2$, differentiate (20) with respect to time and integrate by parts we get:

$$\begin{aligned}
\eta_t &= \int (\partial_s(gT_s) - \nu^2\partial_s(\tilde{T}_s))(T-\tilde{T}) \\
&\quad + \int I_g(T_s - \tilde{T}_s)(T-\tilde{T}) - \frac{1}{2}\int \partial_s(\nu^2)\tilde{T}_s(T-\tilde{T}) \\
&= \int \partial_s(gT_s - \tilde{T}_s)(T-\tilde{T}) + \int (1-\nu^2)\tilde{T}_{ss}(T-\tilde{T}) \\
&\quad + \frac{1}{2}\int I_g\partial_s((T-\tilde{T})^2) - \frac{1}{2}\int \partial_s(\nu^2)\tilde{T}_s(T-\tilde{T}) \\
&= -\int (gT_s - \tilde{T}_s)(T_s - \tilde{T}_s) - \int \partial_s(1-\nu^2)\tilde{T}_s(T-\tilde{T}) \\
&\quad - \int (1-\nu^2)\tilde{T}_s(T_s - \tilde{T}_s) - \frac{1}{2}\int g\kappa^2(T-\tilde{T})^2 \\
&\quad - \frac{1}{2}\int \partial_s(\nu^2)\tilde{T}_s(T-\tilde{T}) \leq -\int g(T_s - \tilde{T}_s)^2 \\
&\quad - \int (g-1)\tilde{T}_s(T_s - \tilde{T}_s) - \int (1-\nu^2)\tilde{T}_s(T_s - \tilde{T}_s)
\end{aligned}$$

$$
\begin{aligned}
&+\frac{1}{2}\int \partial_s(\nu^2)\tilde{T}_s(T-\tilde{T}) \le \int(\nu^2-g)\tilde{T}_s(T_s-\tilde{T}_s)\\
&+\frac{1}{2}\int \partial_s(\nu^2)\tilde{T}_s(T-\tilde{T}) = -\int(\nu^2-g)\tilde{T}_s^2\\
&+\int(\nu^2-g)\tilde{T}_s T_s+\frac{1}{2}\int \partial_s(\nu^2)\tilde{T}_s(T-\tilde{T})\\
\le &\int|\nu^2-g|\tilde{T}_s^2+\int(\nu^2-g)\tilde{T}_s T_s\\
&+\frac{1}{2}\int \partial_s(\nu^2)\tilde{T}_s(T-\tilde{T}) \le \int|\nu^2-g|\tilde{T}_s^2\\
&+\int(\nu^2-g)\tilde{T}_s T_s+\frac{1}{4}P_2(t)\int\tilde{T}_s^2+\frac{1}{4}\eta
\end{aligned}
$$

The last inequality follows from Cauchy's inequality combined with Lemma 6.1, provided that $P_2(t)$ denotes the polynomial of degree 2 given by the bound on $(\partial_s(\nu^2))^2 = (\partial_u(\nu^2)/\nu)^2$. Since s is the arc length, we have that $T_s = \kappa T^{\perp}$, where κ is the curvature of the underlying solution to RCF. Thus, by Proposition 6.3, its L^2-norm is bounded by $\|T_s\|_{L^2}^2 = \|\kappa\|_{L^2}^2 \le \|\kappa(s,0)\|_{L^2}^2 = \|\kappa_0\|_{L^2}^2$. Applying Cauchy-Schwarz to $\int(\nu^2-g)\tilde{T}_s T_s$, it follows that η_t fulfills:

$$
\begin{aligned}
\eta_t &\le \int|\nu^2-g|\tilde{T}_s^2+\|(\nu^2-g)\tilde{T}_s\|_{L^2}\|T_s\|_{L^2}\\
&\le K\|\tilde{T}_s\|_{L^2}^2+K\|\kappa_0\|_{L^2}\|\tilde{T}_s\|_{L^2}\\
&\quad+\frac{1}{4}P_2(t)\|\tilde{T}_s\|_{L^2}^2+\frac{1}{4}\eta
\end{aligned}
$$

where K is a bound on $(g-\nu^2)^2$. Further, because Eq. (18) is of elliptic type with initial condition $T(s,t_0)$ it can be shown that:

$$
\nu_{\min}^2\max_t\left\|\tilde{T}_s\right\|_{L^2}^2 \le \max_t\left\|g\kappa^2\right\|_{L^2}^2
$$

These considerations yield that $\eta_t \le \epsilon(C_1\|\kappa_0\|_{L^2}^2 + C_2\epsilon + C_3\epsilon P_2(t)) + C_4\eta$ for suitable constants $C_1 \ldots C_4$. Finally, applying Gronwalls's Lemma we obtain that η is bounded by:

$$
\begin{aligned}
\eta(t) &\le e^{C_4 t}\left(\eta(0)+\epsilon\int_0^t C_1\|\kappa_0\|_{L^2}^2\right.\\
&\qquad\left.+C_2\epsilon+C_3\epsilon P_2(t)dt\right)\\
&\le \epsilon T(C_1\|\kappa_0\|_{L^2}^2+C_2\epsilon+C_3\epsilon P_2(T))e^{C_4 T}
\end{aligned}
$$

That is, it exists a time t_0 ensuring that solutions to (17) and (19) with initial condition $T(s,t_0)$ differ less than ϵ in L^2, for finite times $0 \le t \le T$. Finally, Proposition 5 ensures that solutions to (15) and (16) computed over the parameter u also converge to each other in the latter sense since:

$$
\begin{aligned}
\eta(s,t) &= \int(T(s,t)-\tilde{T}(s,t))^2 ds\\
&= \int(T(u,t)-\tilde{T}(u,t))^2\nu(u,t)\,du\\
&\ge \nu_{\min}\eta(u,t)
\end{aligned}
$$

This asymptotic behavior, yields the following:

$$
\begin{aligned}
\|\tilde{T}_\rho - T\|_{L^2} &= \|\tilde{T}(\rho)-T(t)\|_{L^2} \le \|\tilde{T}(\rho)\\
&\quad -T(\rho+t)\|_{L^2}+\|T(\rho+t)-T(t)\|_{L^2} \overset{t\to\infty}{\longrightarrow} 0
\end{aligned}
$$

The first summand converges to zero because $T(\rho+t)$ is the solution to (17) for initial condition $T_0 = T(s,t)$ at time $t=\rho$. Hence, $\|\tilde{T}(\rho)-T(\rho+t)\|_{L^2} = \eta(\rho) \le \epsilon$, if t is large enough. The second, because solutions to Eq. (17) are Cauchy, as they converge to a curve in time. □

Remark. We would like to clarify that the proof of the former Proposition does not mean that $T(u,t)$ solves the heat equation in the limit (this would imply convergence to a trivial state!). It rather points out that the soultion to the heat equation:

$$
\tilde{T}_t = \tilde{T}_{uu} \quad \text{with} \quad \tilde{T}(u,0) = T(u,t_0) \qquad (21)
$$

is a sort of first order approximation of $T(u,t)$, in the sense that, if we note by $\tilde{T}^{t_0} = \tilde{T}(0,\rho,t_0)$ the solution to (21) for times $0 \le t \le \rho$, then the collection of functions $\{\tilde{T}^{t_0}, \tilde{T}^{t_0+\rho}, \ldots, \tilde{T}^{t_0+n\rho}\ldots\}_n$ approximates $T(u,t)$ for times, t_0, large enough.

Acknowledgments

This work was partially supported by the project TIC2000-1635-C04-04 of CICYT, Ministerio de Ciencia y Tecnología of Spain.

References

1. L. Alvarez, F. Guichart, P.L. Lions, and J.M. Morel, "Axioms and fundamental equations of image processing," *Arch. Ration. Mech. and Anal.*, Vol. 123, pp. 199–257, 1993.

2. G. Aubert, M. Barlaud, L. Blanc-Feraud, and P. Chatbonnier. "Deterministic edge-preserving regularization in computer imaging," *IEE Trans. Imag. Process.*, Vol. 6, No. 2, 1997.
3. F. Catt, P.-L. Lions, J.-M. Morel, and T. Coll, "Image selective smoothing and edge detection by nonlinear image diffusion," *SIAM J. Num. Ana*., Vol. 29, pp. 182–193, 1992.
4. Y.G. Chen, Y. Giga, and S. Goto, "Uniqueness and existence of viscosity solutions of generalized mean curvature flow equations," *J. Differential Geometry*, Vol. 33, pp. 749–786, 1991.
5. C.K. Chui, An introduction to Waveletes, *Wavelet Analisys and its Applications*, Academic Press, INC., 1992.
6. M.G. Crandall, H. Ishii, and P.L. Lions, "User's guide to viscosity solutions of second order partial differential equations," *Bulletin of the American Math. Society*, Vol. 27, pp. 1–67, 1992.
7. L.C. Evans, "Partial differential equations," Berkeley Mathematics Lecture Notes, Vol. 3B, 1993.
8. M. Gage and R.S. Hamilton, "The heat equation shrinking convex plane curves," *J. Differential Geometry*, Vol. 23, pp. 69–96, 1986.
9. D. Gil and P. Radeva, "Regularized curvature flow," Comp. Vision Center Tech. Report n 63, 2002.
10. M.A. Grayson. "The heat equation shrinks embedded plane curves to round points," *J. Differential Geometry*, Vol. 26, pp. 285–314, 1986.
11. B. Kimia and K. Siddiqi, "Geometric heat equation and non linear diffusion of shapes and images," in *CVPR'94*, 1994.
12. B. Kimia, A. Tanenbaum, and S.W. Zucker, "Toward a computational theory of shape: An overwiew," *Lecture Notes in Comp. Sci*., Vol. 427, pp. 402–407, Springer-Verlag: New York-Berlin, 1990.
13. B. Kimia, A. Tanenbaum, and S.W. Zucker, "On the evolution of curves via a function of curvature I: The classical case," *J. Math. Analysis and Aplications*, vol. 163, pp. 438–458, 1992.
14. R. Malladi and J.A. Sethian, "Image processing: Flows under min-max curvature and mean curvature," *GMIP*, Vol. 58, No. 2, pp. 127–141, 1996.
15. R. Malladi, J.A. Sethian, and B.C. Vemuri, "Shape modeling with front propagation: A level set approach," *PAMI*, Vol. 17, No. 2, pp. 158–175, 1995.
16. Mallat, *A Wavelet Tour of Signal Processing*, Academic Press, Inc., 1999.
17. J. Monteil and Azeddine Beghdadi, "A new interpretation an improvement of the nonlinear anisotropic diffusion for image enhancement," *IEEE Trans. IP*, Vol. 21, No. 9, 1999.
18. S.J. Osher and J.A. Sethian "Front propagation with curvature dependent speed: Algorithms based on Hamilton-Jacobi formulations," *Journal of Computational Physics*, Vol. 79, pp. 12–49, 1988.
19. P. Perona and J. Malik, "Scale space and edge detection using anisotropic diffusion," in *Proc. IEEE Comp. Soc. Workshop on Comp. Vision*," IEEE Computer Society Press, pp. 16–22, 1987.
20. G. Sapiro, *Geometric Partial Differential Equations and Image Analysis*, Cambridge University Press: Cambridge, U.K., 2001.
21. J.A. Sethian, *Level Set Methods: Evolving Interfaces in Geometry, Fluid Mechanics, Computer Vision and Material Sciences*, Cambridge Universirty Press: Cambridge, U.K., 1996.
22. M. Spivak, *A Comprehensive Introduction to Differential Geometry*, Houston: Publish or Perish, Cop. 1979.
23. J. Weickert, "Anisotropic diffusion in image processing," PhD Thesis, Jan. 1996.
24. J. Weickert, "A review of nonlinear diffusion filtering," in Scale-Space Theory in Computer Vision, B. Haar Romery, l. Florack, J. Koenderink, and M. Viergever (Eds.), Lecture Notes in Computer Science, Vol. 1252, Springer-Verlag: Berlin, 1997, pp. 3–28.
25. J. Weickert and B. Benhamouda, "A semidiscrete nonlinear scale-space theory and its relation to the Perona-Malik paradox," in *TFCV '96*, F. Solina, W.G. Kropatsch, and R. Klette, R. Bajcsy (Eds.), Springer-Verlag, Wien, 1997.
26. J. Weickert, B.M. ter Haar Romeny, and M.A. Viergever, "Efficient and reliable schemes for nonlinear diffusion filtering," *IEEE Trans. IP*, 1998.
27. Y.-L.You and M. Ka veh, "Formation of step images during anisotropic diffusion," in *ICIP '97*, 1997.
28. Y.-L.You, W. Xu, A.Tannenbaum, and M. Ka veh, "Behavioral analysis of anisotropic diffusion in image processing," *IEEE Trans. IP*, 1996.

Dèbora Gil has received her Bachelor degree in Pure Mathematics at the University of Barcelona (UB), Spain in 1995. She received her BSC in the area of Geoemetry and Topology at the Mathematical Department of the Universitat AutÚnoma de Barcelona (UAB) in 1998. In 1999 she joined the Computer Science Department of the Universitat AutÚnoma de Barcelona (UAB), where she is currently a PhD student. Her interests are the study of partial differential equations from a geometric point of view, with especial emphasis in the design of geometric flows and deformable models for image processing.

Petia Radeva has received her Bachelor degree in Applied Mathematics and Computer Science at the University of Sofia, Bulgaria in 1989. She joined the Computer Science Department of the Universitat AutÚnoma de Barcelona (UAB) in 1991 as a teaching professor. In 1993 she received the Ms. Sci degree and in 1998 she received the Ph.D. at the UAB on work in development of physics-based models applied to image analysis. Currently, Petia Radeva is a teaching

professor in the Computer Science Department of the Universitat AutÚnoma de Barcelona. Petia Radeva has been and is principal researcher and co-ordinator of several national and european research and industrial projects related to computer vision technologies. She has more than 60 international publications in international journals and proceedings in the field of Medical Imaging, Image Segmentation, Pattern Recognition and Computer Vision. Her present research interests are concentrated on development of physics-based approaches (in particular statistics methods and deformable models) for medical image analysis, industrial vision and remote sensing.